A&A 489, L57–L60 (2008)
DOI: 10.1051/0004-6361:200810719

Astronomy & Astrophysics

Letter to the Editor

Chromospheric magnetic field and density structure measurements using hard X-rays in a flaring coronal loop

E. P. Kontar[1], I. G. Hannah[1], and A. L. MacKinnon[2]

[1] Department of Physics and Astronomy, University of Glasgow, G12 8QQ, UK
e-mail: [eduard;iain]@astro.gla.ac.uk
[2] Department of ACE, University of Glasgow, G12 8QQ, UK
e-mail: alec@astro.gla.ac.uk

Received 30 July 2008 / Accepted 26 August 2008

ABSTRACT

Aims. A novel method of using hard X-rays as a diagnostic for chromospheric density and magnetic structures is developed to infer sub-arcsecond vertical variation of magnetic flux tube size and neutral gas density.
Methods. Using Reuven Ramaty High Energy Solar Spectroscopic Imager (RHESSI) X-ray data and the newly developed X-ray visibilities forward fitting technique we find the *FWHM* and centroid positions of hard X-ray sources with sub-arcsecond resolution (~0.2″) for a solar limb flare. We show that the height variations of the chromospheric density and the magnetic flux densities can be found with an unprecedented vertical resolution of ~150 km by mapping 18−250 keV X-ray emission of energetic electrons propagating in the loop at chromospheric heights of 400−1500 km.
Results. Our observations suggest that the density of the neutral gas is in good agreement with hydrostatic models with a scale height of around 140 ± 30 km. *FWHM* sizes of the X-ray sources decrease with energy suggesting the expansion (fanning out) of magnetic flux tubes in the chromosphere with height. The magnetic scale height $B(z)\,(\mathrm{d}B/\mathrm{d}z)^{-1}$ is found to be of the order of 300 km and a strong horizontal magnetic field is associated with noticeable flux tube expansion at a height of ~900 km.

Key words. Sun: chromosphere – Sun: flares – Sun: X-rays, gamma rays – Sun: magnetic fields – Sun: activity

1. Introduction

Chromospheric magnetic fields are notoriously difficult to measure and their detailed structure is effectively inaccessible with modern observations. The difficulties of various line spectroscopic techniques (e.g. Solanki et al. 2006) occur because the magnetic field is relatively weak, so the observed spectral lines are consequently broad and insensitive to the field. The computation of chromospheric vector magnetic fields from spectral lines is also an ill-conditioned inverse problem (e.g. Metcalf et al. 1995). In addition, current ground based vector magnetograms have a spatial resolution comparable to the vertical size of the chromosphere itself, 2−3″ (Lagg 2007). Therefore, various indirect techniques are often employed to determine the magnetic field in the chromosphere: optical observations of photospheric magnetic fields combined with extrapolation into the chromosphere (e.g. McClymont et al. 1997) or radio observations of gyroresonance emission (Lang et al. 1993; Aschwanden et al. 1995; Vourlidas et al. 1997; White & Kundu 1997).

The solar chromosphere being only about 2000 km thick (~3″) strategically covers the layer where the solar atmosphere turns from the gas-dominated lower chromosphere/photosphere into the magnetic field dominated upper chromosphere/corona. Gabriel (1976) has proposed that the magnetic field in the chromosphere fans out (canopies) and Giovanelli & Jones (1982) have found that the canopy height should be typically 300−400 km. However, polarisation measurements by Landi degl'Innocenti (1998) suggest a very small horizontal component of the magnetic field and Schrijver & Title (2003) argue that the "wine-glass" shaped magnetic field should return to the photosphere near their parent flux tube. In addition, different magnetic field models predict different canopy heights (Solanki et al. 1999).

The transport of both thermal and energetic charged particles in the solar atmosphere is governed by individual magnetic flux tubes. Therefore flare accelerated electrons one-dimensionally propagating along magnetic field lines can trace individual flux tubes from the electron acceleration site in the corona down to the deep layers of chromosphere where electrons emit hard X-ray emission. The asymmetry of hard X-ray footpoint sizes of a flaring loop (Melrose & White 1979) could be a measure of the ratio of magnetic field strengths in the X-ray loop footpoints (Schmahl et al. 2007). The simple dependency of the X-ray emission maximum location on the photon energy and density structure in the low corona/chromosphere due to Coulomb collisions (Brown et al. 2002), has allowed Aschwanden et al. (2002) to infer the chromospheric density structure from Reuven Ramaty High Energy Solar Spectroscopic Imager RHESSI (Lin et al. 2002) X-ray observations.

In this letter, we show that X-rays can be a diagnostic tool for the analysis of not only energetic electrons in solar flares but of the magnetic flux tubes and density structure in the chromosphere. We analyse the spatial and energy distribution of hard X-ray sources using RHESSI data to infer chromospheric density and magnetic field structure. Our results show that the density distribution of neutral hydrogen in the flaring loop has a scale height of 140 km and the magnetic flux tube of the flaring loop fans out by a factor of ~3 at the height of around 900 km.

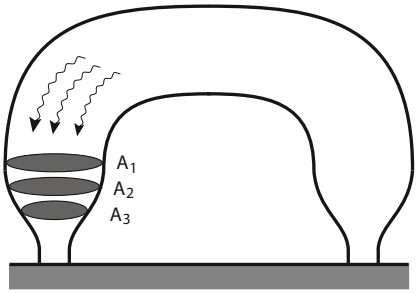

Fig. 1. Cartoon of a magnetic loop and electron precipitation along the loop. The spatial size of the X-ray emission decreases with height, indicating the changing magnetic loop width.

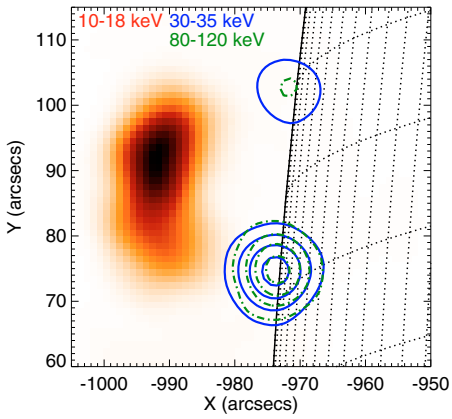

Fig. 2. RHESSI CLEAN (Hurford et al. 2002) X-ray images of the January 6, 2004 limb event. The contours show hard X-ray emission integrated for the impulsive phase of the flare (06:22:20–06:23:00 UT) from the footpoints in 30–35 keV (solid blue line) and 80–120 keV (dot-dashed green lines) ranges. The background image shows subsequent softer thermal emission (06:24:00–06:24:40 UT) in 10–18 keV range.

2. Electron precipitation in magnetic loops

Accelerated electrons follow magnetic field lines towards the denser layers of the atmosphere, losing energy to binary collisions and scattering in angle en route. In the first instance we follow Brown et al. (2002) and neglect scattering. Then the flux $F(E,z)$ (electrons s^{-1} cm^{-2} keV^{-1}) of electrons of energy E at depth z from the acceleration point $z = 0$, is

$$F(E,z) = F_{\rm IN} E \left(\sqrt{E^2 + 2KN(z)} \right)^{-\delta-1}, \quad (1)$$

where $N(z)$ is the column depth $N(z) = \int_0^z n(z)\mathrm{d}z$, $K = 2\pi e^4 \ln\Lambda$, e is the electron charge, $\ln\Lambda$ is the Coulomb logarithm (Brown 1973; Kontar et al. 2002) and we have assumed an injected flux of accelerated electrons $F(E, z = 0) = F_{\rm IN} E^{-\delta}$ (electrons keV^{-1} cm^{-2} s^{-1}) at $z = 0$. The hard X-ray flux from depth z is

$$I(\epsilon,z) = \frac{n(z)}{4\pi R^2} \int_\epsilon^\infty F(E,z)\sigma(\epsilon,E)\mathrm{d}E \quad (2)$$

where ϵ is the photon energy and $\sigma(\epsilon, E)$ is isotropic bremsstrahlung cross-section (Haug 1997). Since the density $n(z)$ increases with z while the electron flux $F(E,z)$ decreases, $I(\epsilon,z)$ thus exhibits a maximum for a fixed ϵ at a depth $z_{\rm max}(\epsilon)$ that increases monotonically with ϵ (Brown et al. 2002). Lower energy electrons lose their energy faster, with higher energy electrons propagating deeper into the atmosphere and the higher energy X-ray emission should come from lower layers of the solar atmosphere.

If the magnetic field strength $B(z)$ increases with depth (Fig. 1), the cross-sectional area $A(z)$ of the flux tube will obey the principle of magnetic flux conservation $B(z)A(z) = \text{const.}$ (e.g. Melrose & White 1979). The size of the X-ray source at energy ϵ becomes a measure of $A(z)$ at $z_{\rm max}(\epsilon)$ for limb events (Fig. 1), which are unaffected by albedo effects (Kontar et al. 2006). We assume in the first instance that the electrons move parallel to the field so they experience no mirror force although $B(z)$ varies. Electrons contributing most to radiation at $z_{\rm max}(\epsilon)$ will still be close to their initial energies and thus mostly still moving along their initial directions (Brown 1972; Leach & Petrosian 1981; MacKinnon & Craig 1991).

3. RHESSI X-ray observations

We selected a large GOES M6 class X-ray flare that appeared at the eastern limb on January 06, 2004 with a hard X-ray peak at ~06:23 UT. The flare has an extended coronal source visible in soft X-rays and two hard X-ray footpoints (Fig. 2). The "southern" footpoint is 5–10 times stronger than the northern footpoint, which seems partially occulted at energies above ~120 keV. This flare seems ideal for our analysis since it is a limb event with one dominant source of hard X-ray emission seen in images up to ~300 keV. In addition, the spatially integrated count rate suggests emission above 800 keV. The spatially integrated photon spectrum for the same time interval (06:22:20–06:23:00 UT) has been fitted using an isothermal plus thick-target model (Fig. 3). The X-ray emission above 18 keV (Fig. 3) is dominated by the footpoint thick-target emission and can be used for our analysis. At these energies the "southern" X-ray source is the brightest and is used for detailed imaging analysis in different energy ranges.

X-ray visibilities (2-dimensional spatial Fourier components) (see Schmahl et al. 2007) in ten different hard X-ray energy ranges from 18 to 250 keV have been forward fitted using a single circular Gaussian source (Fig. 3). Although the figure shows the fitted source matching the imaged footpoint location, the fit has been conducted on the X-ray visibilities from which the images are derived, not the images themselves. The X-ray images per se are generally a poor indicator of the source size (Hurford et al. 2002; Emslie et al. 2003). Visibility forward fit however provides reliable spatial measures and clear statistical uncertainties for all the fit parameters. These fits provided us with the centroid positions of the Gaussian source ($x(\epsilon)$, $y(\epsilon)$), and its Full Width at Half-Maximum ($FWHM$) size $s(\epsilon)$. Assuming a vertically emerging magnetic field and calculating the radial distance measured from the disk centre of the Sun $R(\epsilon) = \sqrt{x(\epsilon)^2 + y(\epsilon)^2}$ we can readily find the height of the X-ray source $h(\epsilon) = R(\epsilon) - R_0$, where R_0 is the radial distance of the bottom of the loop. The typical uncertainties on radial distance measurements $R(\epsilon)$ are around $0.2'' \sim 150$ km. R_0 is poorly known (Aschwanden et al. 2002) but is crucial for the detailed analysis, therefore we incorporate it as a fit parameter. We assume the neutral hydrogen density profile to be

$$n(h(\epsilon)) = n_0 \exp\left(-(R(\epsilon) - R_0)/h_0\right) \quad (3)$$

where h_0 is the density scale height, and n_0 is the number density at height $h = 0$. Various chromospheric models A-F from Vernazza et al. (1981) provide slightly different values of n_0 though most are very close to $n_0 = 1.16 \times 10^{17}$ cm^{-3}. Therefore

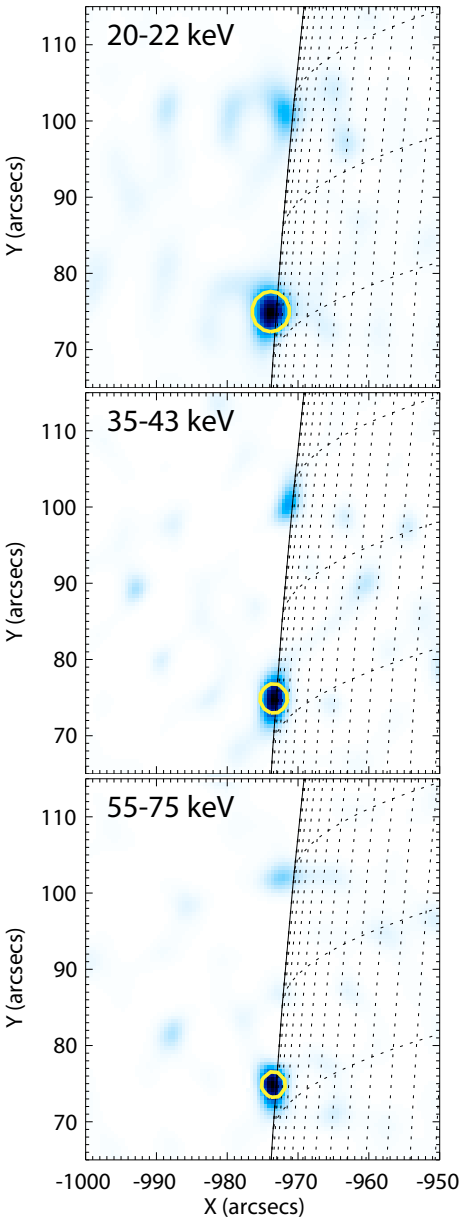

Fig. 3. RHESSI MEM NJIT (Schmahl et al. 2007) images in 3 energy ranges (*top to bottom*: 20–22 keV, 35–43 keV, 55–75 keV) integrated for the impulsive phase of the flare (06:22:20–06:23:00 UT). The *FWHM* circular source size found by forward fitting the X-ray visibilities, which were also used to make the background images, are shown by the overplotted contours (orange lines).

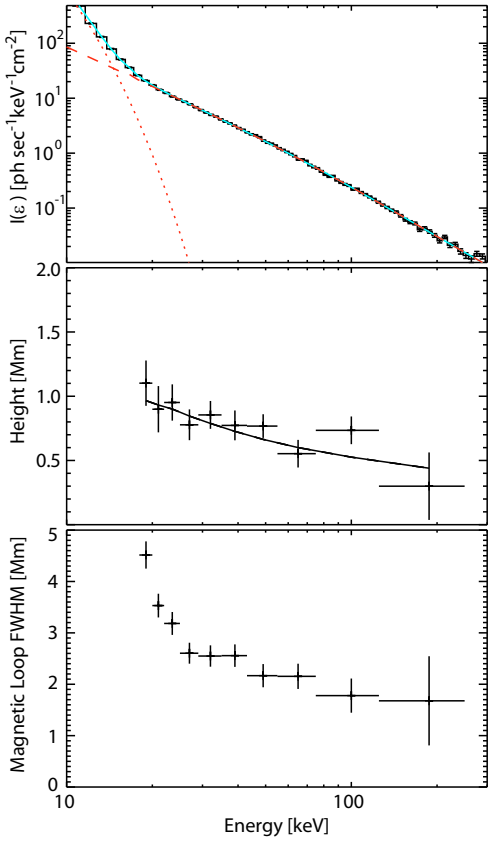

Fig. 4. *Top*: spatially integrated RHESSI X-ray spectrum (histogram) of the flare's impulsive phase (06:22:20–06:23:00 UT) fitted with an iso-thermal plus thick target model fit (solid line). The fit provides a temperature 1.65 keV (19 MK), emission measure 2×10^{48} cm^{-3} (dotted lines) and spectral indices $\delta = 3.2$ below 191 keV and 3.9 above. *Middle*: "Southern" hard X-ray source height as a function of energy, $h(\epsilon) = R(\epsilon) - R_0$, where $R_0 = 975.3''$. *Bottom*: *FWHM* circular source size as a function of energy.

we use this n_0 as a boundary condition to find the characteristic scale-height as well as R_0. Using Eq. (3) to fit the maximum of the flux spectrum given by Eq. (2) with $\ln \Lambda = \ln \Lambda_{eH} = 7.1$ (Brown 1973; Kontar et al. 2002) and using the spectral index found from the spatially integrated spectrum $\delta = 3.2$ (top panel Fig. 4) we find $R_0 = 975.3 \pm 0.2''$ and $h_0 = 140 \pm 30$ km. Using these fitted parameters we can now plot the centroid height h against energy (Fig. 4, middle panel), with the fitted model overplotted, finding that the height decreases by less than 500 km between 20 keV and ~200 keV.

The *FWHM* sizes $s(\epsilon)$ of the source, found from forward fitting the visibilities, decrease with energy from $6.2''$ (4.5 Mm) to $2.3''$ (1.7 Mm) (Fig. 4, bottom panel). Estimation of the magnetic field structure and density structure is shown in the top and bottom panels of Fig. 5 respectively. We find that the magnetic field structure widens with increasing height and that the density decreases by over 2 orders of magnitude from a height of 1 Mm above the photosphere.

4. Discussion and conclusions

Forward fitting X-ray visibilities allow simple and reliable measurements of not only locations of the emission maxima but also the characteristic sizes of hard X-ray sources. By using this visibility analysis on a good candidate limb flare we have substantially improved the earlier chromospheric height and density measurements of Aschwanden et al. (2002), reducing the uncertainty of emission maximum positions to ~$0.2''$. Assuming collisional transport in neutral hydrogen it can be concluded that the chromospheric density is consistent with a gravitationally stratified atmosphere of density scale height 140 ± 30 km. We show for the first time that not only is the higher energy X-ray emission produced continuously deeper in the chromosphere but the X-ray source sizes decrease from ~$6.2''$ to ~$2.3''$. The precise measurement of the characteristic sizes allows us to conclude that the magnetic field directing the energetic electrons converge, with the magnetic flux tube shrinking from *FWHM* ~ 3.5 Mm at $h \sim 1$ Mm to *FWHM* ~ 2.5 Mm at $h \sim 0.8$ Mm above the photosphere. The magnetic scale height estimated

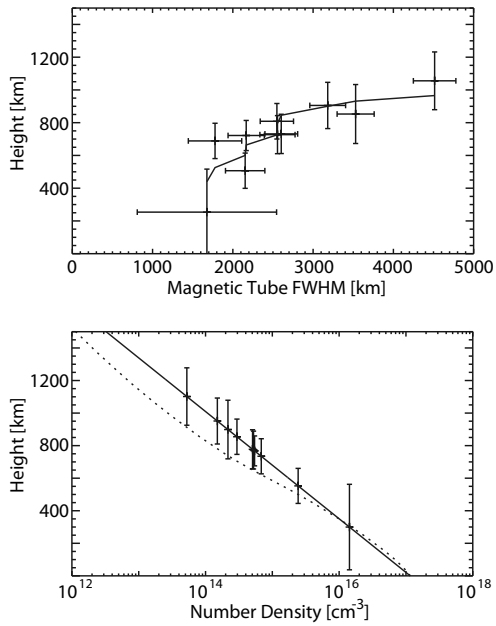

Fig. 5. *Top*: chromospheric magnetic flux tube *FWHM* at various heights with *FWHM* for the density fit given by Eq. (3) (solid line). *Bottom*: the chromospheric neutral number hydrogen density as a function of height; best fit with the neutral gas density profile given by Eq. (3) (solid line), density model C from Vernazza et al. (1981) (dashed line).

using flux conservation $B(h) \sim FWHM(h)^{-2}$ as the ratio of areas $B(h)\,(\mathrm{d}B/\mathrm{d}h)^{-1} = -FWHM(h)\mathrm{d}h/\mathrm{d}FWHM(h)/2$ is found to be of the order of 300 km. This confirms the fanning out (canopies) of the chromospheric magnetic fields (Gabriel 1976).

Our deduced density structure agrees quite well with independent estimations from other methods, possibly a surprising conclusion in view of the simple treatment of electron transport, completely neglecting any pitch-angle changes. As already noted, collisional scattering will modify the range only by a factor of order unity but magnetic moment conservation might have a greater effect, unless fast electrons all start with velocity vectors parallel to $\boldsymbol{B}$. Large pitch angles would develop via collisional scattering only as electrons reach the end of their ranges, and the mirror force would be similarly unimportant most of the time. Such a concentration at small pitch angles seems at odds with findings of a nearly isotropic electron distribution from studies of photospheric albedo (Kontar & Brown 2006). The magnetic field convergence we find here however offers a simple solution. The flux tube implied by our HXR source *FWHM*s imply magnetic field lines substantially inclined to the vertical, possibly by as much as 60% on average at the outer edge and in addition are likely to be twisted. The HXR polar diagram of electrons populating the whole of an ensemble of field lines, with such a range of angles to the vertical, would be much closer to isotropic than expected for vertical field lines. The presence of magnetic canopies, then, appears to be a critical factor for interpreting HXR images and even spectra, but one that needs a much more substantial and detailed modelling effort than we attempt here.

While the X-ray diagnostics of the chromospheric magnetic field is an extremely attractive new technique, we emphasise that the morphology of X-ray sources should be further scrutinised. We note that the shape of the hard X-ray sources is more elliptical (Fig. 3) rather than circular suggesting that the vertical extent of X-ray sources is governed by the spatially varying magnetic field (convergence and a twist of the flux tube), through the conservation of the electron magnetic moment. This complicates the interpretation of the HXR source sizes beyond the simple ideas embodied in (1) and (2) but brings new diagnostic potential. This requires a more complicated electron dynamic and forward fitting elliptical sources to the X-ray visibilities, which will be the subject of future work.

The method of measuring magnetic field using X-rays can be viewed as a unique tool of loop width measurements in the chromosphere comparable to using TRACE data to measure the widths of flux tubes in the corona (Watko & Klimchuk 2000). While it is often argued that the heights of line formation should not be assigned due to the fact that very distinct layers of the atmosphere could be sampled (e.g. Sanchez Almeida et al. 1996), X-rays are uniquely related to the magnetic field lines connecting the photosphere and the electron injection site in the corona and weakly sensitive (via Coulomb logarithm dependency) to the temperature variations in the chromosphere. Therefore hard X-ray emission is likely to be a valuable diagnostic for mapping chromospheric magnetic field and density structures.

Acknowledgements. This work was supported by a STFC rolling grant (E.P.K., I.G.H., A.L.M.) and STFC/PPARC Advanced Fellowship (E.P.K.). Financial support by the European Commission through the SOLAIRE Network (MTRN-CT-2006-035484) is gratefully acknowledged. The authors are thankful to Markus Aschwanden for useful referee comments.

References

Aschwanden, M. J., Lim, J., Gary, D. E., & Klimchuk, J. A. 1995, ApJ, 454, 512
Aschwanden, M. J., Brown, J. C., & Kontar, E. P. 2002, Sol. Phys., 210, 383
Brown, J. C. 1972, Sol. Phys., 26, 441
Brown, J. C. 1973, Sol. Phys., 28, 151
Brown, J. C., Aschwanden, M. J., & Kontar, E. P. 2002, Sol. Phys., 210, 373
Emslie, A. G., Kontar, E. P., Krucker, S., & Lin, R. P. 2003, ApJ, 595, L107
Gabriel, A. H. 1976, Roy. Soc. of London Phil. Trans. Ser. A, 281, 339
Giovanelli, R. G. & Jones, H. P. 1982, Sol. Phys., 79, 267
Haug, E. 1997, A&A, 326, 417
Hurford, G. J., Schmahl, E. J., Schwartz, R. A., et al. 2002, Sol. Phys., 210, 61
Kontar, E. P. & Brown, J. C. 2006, ApJ, 653, L149
Kontar, E. P., Brown, J. C., & McArthur, G. K. 2002, Sol. Phys., 210, 419
Kontar, E. P., MacKinnon, A. L., Schwartz, R. A., & Brown, J. C. 2006, A&A, 446, 1157
Lagg, A. 2007, Adv. Space Res., 39, 1734
Landi degl'Innocenti, E. 1998, Nature, 392, 256
Lang, K. R., Willson, R. F., Kile, J. N., et al. 1993, ApJ, 419, 398
Leach, J. & Petrosian, V. 1981, ApJ, 251, 781
Lin, R. P., Dennis, B. R., Hurford, G. J., et al. 2002, Sol. Phys., 210, 3
MacKinnon, A. L. & Craig, I. J. D. 1991, A&A, 251, 693
McClymont, A. N., Jiao, L., & Mikic, Z. 1997, Sol. Phys., 174, 191
Melrose, D. B. & White, S. M. 1979, Proc. Astron. Soc. Austr., 3, 369
Metcalf, T. R., Jiao, L., McClymont, A. N., Canfield, R. C., & Uitenbroek, H. 1995, ApJ, 439, 474
Sanchez Almeida, J., Ruiz Cobo, B., & del Toro Iniesta, J. C. 1996, A&A, 314, 295
Schmahl, E. J., Pernak, R. L., Hurford, G. J., Lee, J., & Bong, S. 2007, Sol. Phys., 240, 241
Schrijver, C. J. & Title, A. M. 2003, ApJ, 597, L165
Solanki, S. K., Finsterle, W., Rüedi, I., & Livingston, W. 1999, A&A, 347, L27
Solanki, S. K., Inhester, B., & Schüssler, M. 2006, Rep. Progr. Phys., 69, 563
Vernazza, J. E., Avrett, E. H., & Loeser, R. 1981, ApJS, 45, 635
Vourlidas, A., Bastian, T. S., & Aschwanden, M. J. 1997, ApJ, 489, 403
Watko, J. A. & Klimchuk, J. A. 2000, Sol. Phys., 193, 77
White, S. M. & Kundu, M. R. 1997, Sol. Phys., 174, 31